Experimental and Kinetic Modeling Evidences of a C_7H_6 Pathway in a Rich Toluene Flame

Valéry Detilleux* and J. Vandooren

Laboratoire de Physico-Chimie de la Combustion, Université catholique de Louvain, 1 Place Louis Pasteur, B1348 Louvain-la-Neuve, Belgium

Received: June 25, 2009; Revised Manuscript Received: August 25, 2009

The structure of a laminar, premixed, and one-dimensional toluene−oxygen−argon (9.9 mol % C_7H_8, 44.5 mol % O_2, and 45.6 mol % Ar) flame, with an equivalence ratio of 2 and burning at 36 Torr was analyzed by gas chromatography and molecular beam mass spectrometry (MBMS). Mole fraction profiles of 25 chemical species including permanent gases of combustion and first polycyclic aromatic hydrocarbons as naphthalene, methylnaphthalene isomers, biphenyl, and phenanthrene have been measured. A kinetic model based on recent literature data has been elaborated to compare with measurements. As suggested by recent theoretical studies, benzyl radical (C_7H_7) dissociation into fulvenallene (C_7H_6) + H and the reaction between C_7H_6 and H giving cyclopentadienyl radical and acetylene have been included into the model. A comparison between experimental and predicted flame structures have allowed us to validate the kinetic model for rich toluene combustion. Moreover, MBMS measurements of mole fraction profiles corresponding to *m*/*z* ratios of C_7H_7 and C_7H_6 have permitted a specific validation of the theoretically postulated C_7H_6 pathway in toluene flames.

Introduction

One of the main goals in the area of hydrocarbon combustion is the understanding of the polycyclic aromatic hydrocarbons (PAH) formation. This interest is due to their threat to human health.[1] Indeed, these heavy and stable compounds, formed when incomplete hydrocarbon oxidation occurs, as in motors or industrial processes, are carcinogenic and thought to be molecular intermediates in soot formation.[2] Toluene is considered as a PAH precursor in rich hydrocarbon flames. In order to reduce PAH and soot formation, a detailed understanding of chemical pathways involved in toluene consumption and in PAH growth under rich combustion conditions is necessary. Such a comprehension can be reached by an extensive analysis of kinetic models able to reproduce experimental evidence.

Whereas many groups studied rich benzene combustion and oxidation, only few works were devoted to toluene. Its oxidation was numerically and experimentally studied at high temperature in a turbulent flow reactor by Venkat, Emdee, and Brezinsky and co-workers[3–6] and in a jet stirred reactor by Dagaut and co-workers[7] and Bounaceur and co-workers.[8] Shock tube experiments were also performed by a few groups.[8–12] Surprisingly, toluene combustion has been poorly investigated in flames.[13–15] To our best knowledge, the very recent work of Li and co-workers[15] is the only in the field of laminar, one-dimensional, and premixed pure toluene flames. Authors have extensively analyzed the structure of a toluene−oxygen−argon flame with an equivalence ratio of 1.9 by tunable synchrotron vacuum ultraviolet photoionization mass spectrometry. However, a kinetic model has not been proposed to predict their experimental results.

Since the benzyl radical (b-C_7H_7) is a major intermediate in toluene combustion, its decomposition pathways have been subject to recent theoretical studies.[16,17] Analyzing the b-C_7H_7 potential energy surface, these works have postulated a pathway linking toluene to the cyclopentadienyl radical through a C_7H_6 intermediate: fulvenallene. Moreover, studying toluene pyrolysis Colket and Seery[12] found that benzyl radical participates to naphthalene ($C_{10}H_8$) formation by reaction with a propargyl radical (C_3H_3). Surprisingly, all of these findings were never validated by kinetic modeling against an experimental toluene−oxygen−argon flame structure.

Regarding the poor experimental database on laminar, premixed, and one-dimensional toluene flames and the need for testing new theoretical findings on benzyl radical decomposition, the measurement of a rich toluene−oxygen−argon flame structure and the development of a kinetic model including recent literature was necessary.

Experimental Methods

Mole fraction profiles of 23 chemical species have been measured by gas chromatography (GC). High purity toluene (99.5%), oxygen (99.5%), and argon (99.99%) were used to prepare the initial gas mixture. GC measurements were performed with the experimental setup shown in Figure 1. It consists of a combustion chamber where a flat flame is stabilized at low pressure (36 Torr) on a movable flat flame burner of 8 cm in diameter. In front of the burner is the apex of a conical quartz nozzle with a 45° angle within 2 cm and with a small hole of 0.2 mm. This nozzle and the movable burner allow sampling to be performed at different heights of the flame.

According to their vapor pressure, chemical species detected in the flame are divided into 2 classes. The first consists of permanent gases of combustion (O_2, CO_2, H_2O, CO, H_2) and high vapor pressure hydrocarbons from C_1 to C_6 while the second includes lower vapor pressure hydrocarbons from C_7 to PAH. Each class is injected into the Gas Chromatograph using a particular setup. High vapor pressure of first class compounds allows us to increase concentration of samples by compressing them before their injection in the GC without condensing constituents (Figure 1). To prevent larger hydrocarbons of second class condensing into the vessel, a second setup is connected at the exit of the quartz nozzle (Figure 2) to heat samples at 200 °C at low pressure (30 mbar), from sampling

* Corresponding author: E-mail address: valery.detilleux@uclouvain.be, Telephone: +32 10 61 47 27 61, Fax: +32 10 61 47 24 68.

10.1021/jp905954g CCC: $40.75
Published on Web 09/18/2009

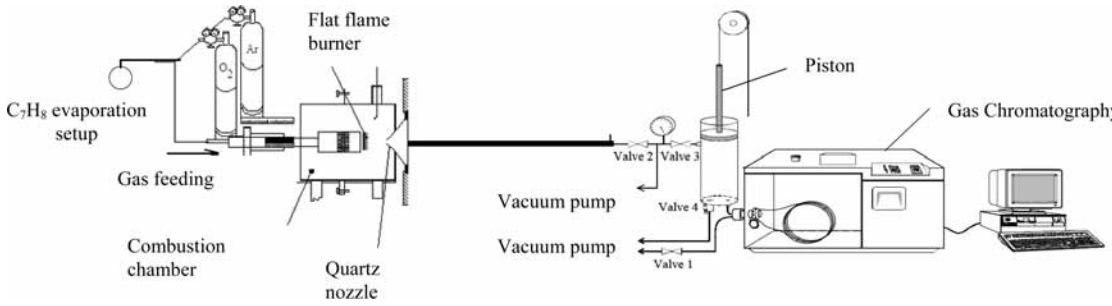

Figure 1. Experimental setup used for C_1 to C_6 and permanent gases of combustion measurements.

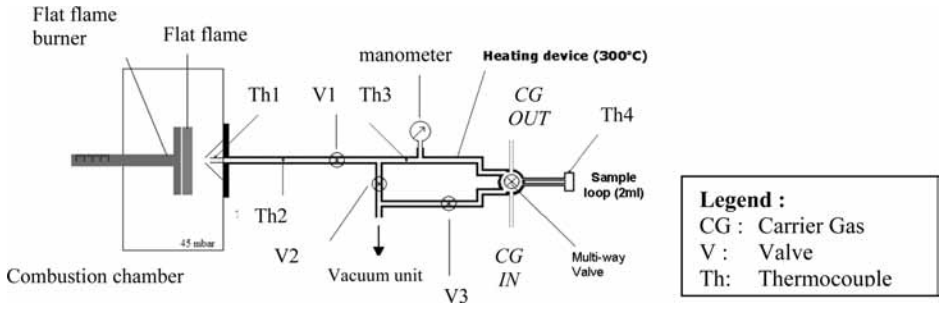

Figure 2. Experimental setup used for C_7 to C_{14} measurements.

until GC injection in order to ensure their gaseous state. The first class compounds chromatographic separation is carried out by a MOLSIEVE 5A and a PORA PLOT Q columns (from Varian inc.) for permanent gases of combustion and hydrocarbons, respectively. Second class chemical species are separated by a CPSIL PAH CB column from Varian inc. Quantitative detection is achieved by a thermal conductivity detector (TCD) and a flame ionization detector (FID) connected in series. Their responses are calibrated for permanent gases of combustion and a large range of stable hydrocarbons, including those observed into the flame. The calibration procedure is divided into two phases. The first consists of measuring molar response factors α_i (see eq 1) of a detector for each compound i by measuring its chromatographic signal I_i for samples of variable quantities of mole (n_i). Samples are injected directly into the gas chromatograph with a syringe. According to its vapor pressure, each compound i is injected either in the gaseous state (CH_4, C_2H_2, etc) or in the liquid state (H_2O) or diluted in an appropriate solvent ($C_{10}H_8$, $C_{12}H_8$, $C_{12}H_{10}$, etc).

$$I_i = n_i \cdot \alpha_i \tag{1}$$

However, in this work it is more adequate to perform a mole fraction calibration than a molar one. Then, if in eq 1 we respectively divide n_i and multiply α_i by the total mole number (n_t) injected by using setups with or without sample compression (illustrated in Figures 1 and 2, respectively), we obtain the eq 2 which links the chromatographic signal intensity (I_i) to the mole fraction χ_i. Since the total molar quantity (n_t) of a sample injected into the GC depends on the type of setup used for its injection, mole fraction response factors β_i have to be determined according to the injection setup used for detection of each compound i.

$$I_i = \left(\frac{n_i}{n_t}\right) \cdot (\alpha_i n_t) = \chi_i \cdot \beta_i \tag{2}$$

The second phase of the calibration consists of measuring these total quantities of mole n_t injected into the GC with both injection setups (illustrated in Figures 1 and 2). Intensity signals corresponding to cold gases mixtures of methane-oxygen-argon with variable compositions were measured using both injection setups in order to determine the mole fraction response factor of methane (β_{CH_4}) with each of them. Then, knowing α_{CH_4} and β_{CH_4}, total molar quantities n_t injected using each setup were calculated from the eq 3.

$$\beta_i = n_t \cdot \alpha_i \tag{3}$$

Since for each injection setup, every sample injection is performed with identical conditions, total quantities of mole (n_t) are constant. Then, the mole fraction calibration factor β_i of any compound i can be calculated from its molar calibration factor α_i and the measured total quantity of mole n_t injected with the setup used for its detection (see eq 3).

Since calibration factors seem linearly correlated to the carbon content of C_xH_y compounds, an accurate approximation can be extrapolated for unstable chemical species such as cyclopentadiene (c-C_5H_6), vinylacetylene (C_4H_4) and diacetylene (C_4H_2). Errors on experimental profiles essentially depend on the reliability of the calibration. Errors of 10% and 20% should be considered for chemical species which are directly calibrated and for unstable compounds, respectively.

Beside gas chromatography, molecular beam mass spectrometry (MBMS) has been used to measure mole fraction profiles of m/z ratios corresponding to C_7H_6 ($m/z = 90$) and C_7H_7 ($m/z = 91$). Indeed, these both chemical species could not be identified by GC and were necessary to validate the kinetic model presented in the next section. The experimental setup used for MBMS measurements is similar to the one used for the gas chromatography analysis (Figure 1) excepted that behind the quartz nozzle, samples are accelerated through differentially pumped chambers toward the ion source of a mass spectrometer. This setup has been extensively described in a previous article.[18]

Mole fractions profiles have been deduced from mass signals measurements by means of the sensitivity factors S_i which link

the signal intensity I_i to the mole fraction χ_i for each chemical species i at a given temperature (eq 4).

$$I_i = S_i \cdot \chi_i \tag{4}$$

Mahnen has shown that for all chemical species sensitivity factors vary in the same manner with the temperature.[19] Therefore, for 2 chemical species i and j, the ratio S_i/S_j is constant all along the flame. So, we can deduce mole fraction (χ_i) profiles for each species by solving the following eq 5:

$$\chi_i = \frac{S_{\text{toluene}}}{S_i} \cdot \frac{I_i}{I_{\text{toluene}}} \cdot \chi_{\text{toluene}} \tag{5}$$

where I_i and I_{toluene} are mass signals measured by MBMS for the species i and for toluene, respectively. χ_{toluene} is the toluene mole fraction measured by Gas Chromatography and S_{toluene}/S_i is the sensitivity factors ratio estimated by the additivity of atomic contributions to the ionization cross section through the eq 6:

$$\frac{S_{\text{toluene}}}{S_i} = \frac{(1.8n_C + 0.65n_H + 1.3n_O)_{\text{toluene}}}{(1.8n_C + 0.65n_H + 1.3n_O)_i} \tag{6}$$

where n_C, n_H, and n_O are the number of carbon, hydrogen, and oxygen atoms, respectively.

Temperature measurements at different heights of the flame have been accomplished by using a Pt/PtRh10% thermocouple, 0.1 mm in diameter, coated with a thin layer of Y_2O_3-BeO ceramic to prevent catalytic effects of Pt on chemical reactions occurring in the flame.[20] Data acquired have been corrected for radiation losses by the electrical compensation method.

Numerical Simulation. The kinetic model used in this study is composed of a H_2/O_2 submechanism from Konnov,[21] a C_1-C_4 submechanism from Ristori and co-workers[22] with vinylacetylene reactions from Richter and Howard[23] and a C_5-C_{12} submechanism developed in the present work. A particular attention was paid to consumption and formation reactions of toluene, benzyl and cyclopentadienyl radicals, cyclopentadiene and naphthalene. The kinetic model may be obtained by contacting the authors. Calculations were performed by using the COSILAB software[24] and the experimental temperature profile has been used as an input parameter.

Experimental Results and Discussion

A one-dimensional toluene−oxygen−argon (9.9 mol % C_7H_8, 44.5 mol % O_2 and 45.6 mol % Ar) flame, with an equivalence ratio of 2 and a fresh gases velocity of 40.5 cm s^{-1} at 298 K, was stabilized at 36 Torr on the flat flame burner of the experimental setup described in Figure 1. The experimental temperature profile is shown in Figure 3. The flame reaches its maximum temperature of 1743 K at 1.05 cm from the burner surface. The following discussion compares the experimental flame structure with data from the numerical simulation and presents the main reaction routes of C_7H_8 rich combustion determined by a comparative reaction rates analysis of the predicted flame structure. The most important reactions are numbered and their kinetic parameters are presented in Table 1.

1. Main Species Formation and Toluene Consumption. Mole fraction measurements of main chemical species are generally well reproduced by the modeling study (Figures 4 and 5). At 1.03 and 1.12 cm above the burner surface reactants C_7H_8 and O_2 are completely consumed, respectively. In the burned gases only few compounds subsist in relatively high concentrations: CO, CO_2, H_2O, H_2 and C_2H_2. Acetylene (C_2H_2) is a major intermediate in toluene combustion and persists in the burned gases. As shown in figure 4, this observation is well predicted by the kinetic modeling. Main pathways of C_7H_8 combustion determined by a comparative reactions rate analysis are summarized in scheme 1.

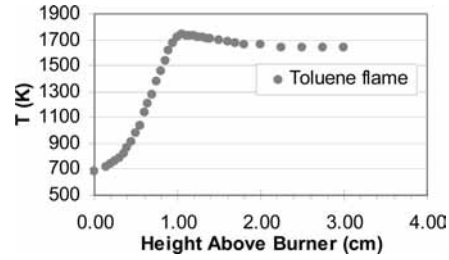

Figure 3. Experimental temperature profile.

C_7H_8 consumption is well predicted by the mechanism and reaches its maximum rate around 0.82 cm from the burner surface. Toluene unimolecular dissociation steps conduct to phenyl and methyl radicals production R1 and to benzyl radical and H atom formation R2.

$$C_7H_8 = C_6H_5 + CH_3 \tag{R1}$$

$$C_7H_8 = b\text{-}C_7H_7 + H \tag{R2}$$

Since benzyl and phenyl radicals are resonantly stabilized, reactions R1 and R2 are energetically favored and play a key role in toluene decomposition. Moreover, phenyl radical has been experimentally identified by many groups[11,12] as a major product of the thermal decomposition of toluene, showing that reaction R1 should not be neglected. Then the use of an adequate branching ratio for these reactions in kinetic modeling of toluene combustion is necessary. Rate constant parameters of reactions R1 and R2 are respectively taken from the work of Lifshitz and co-workers[25] and calculated from the branching ratio deduced from the theoretical master equation analysis of Eng and co-workers.[26]

According to the pathway analysis presented in scheme 1, 59% of toluene (C_7H_8) is converted to benzyl radical (b-C_7H_7) through either unimolecular dissociation R2 or H abstraction reactions by H atom R3 and OH radical R4.

$$C_7H_8 + H = b\text{-}C_7H_7 + H_2 \tag{R3}$$

$$C_7H_8 + OH = b\text{-}C_7H_7 + H_2O \tag{R4}$$

$$C_7H_8 + H = C_6H_6 + CH_3 \tag{R5}$$

23% of toluene dissociates to phenyl and methyl radicals R1 and 18% reacts with H atom to lead to benzene and methyl radical R5. Both of these reactions (R1 and R5) are responsible for 45% of methyl radical formation which is the main precursor of methane (CH_4), very accurately predicted by the kinetic model (Figure 6).

TABLE 1: Kinetic Parameters of Reactions Involved in Paths A and B of Toluene Consumption (See Figure 6), in Naphthalene Formation (See Figure 11) and in Styrene and Phenylacetylene Production

reactions		$k = AT^n \exp(-E_a/RT)$ units: mol, s, cm^3			refs
		A	n	E_a cal/mol	
$C_7H_8 = C_6H_5 + CH_3$	(R1)	5.00×10^{16}	0.00	98000	25
$C_7H_8 = b\text{-}C_7H_7 + H$	(R2)	2.50×10^{14}	0.00	77800	*a*
$C_7H_8 + H = b\text{-}C_7H_7 + H_2$	(R3)	1.30×10^{14}	0.00	8373	40
$C_7H_8 + OH = b\text{-}C_7H_7 + H_2O$	(R4)	1.81×10^{5}	2.39	–600	41
$C_7H_8 + H = C_6H_6 + CH_3$	(R5)	5.78×10^{13}	0.00	8090	42
$C_6H_6 + H = C_6H_5 + H_2$	(R6)	6.02×10^{8}	1.81	16400	43
$C_6H_6 + OH = C_6H_5 + H_2O$	(R7)	2.39×10^{4}	2.68	773	41
$C_6H_6 + O = C_6H_5 + OH$	(R8)	6.00×10^{13}	0.00	11064	*b*
$C_6H_6 + OH = C_6H_5OH + H$	(R9)	1.32×10^{2}	3.25	5590	41
$C_6H_6 + O = C_6H_5O + H$	(R10)	6.66×10^{12}	0.00	2332	*b*
$C_6H_5 + O_2 = C_6H_5O + O$	(R11)	1.02×10^{13}	0.00	3581	27
$C_6H_5 + O_2 = C_6H_4O_2 + H$	(R12)	4.52×10^{12}	0.00	3604	27
$C_6H_5O = c\text{-}C_5H_5 + CO$	(R13)	2.51×10^{11}	0.00	43900	46
$b\text{-}C_7H_7 \rightarrow C_7H_7$	(R14)	4.00×10^{14}	0.00	72000	*c*
$C_7H_7 \rightarrow b\text{-}C_7H_7$	(R15)	5.50×10^{12}	0.00	8700	28
$C_7H_7 \rightarrow C_7H_6 + H$	(R16)	3.70×10^{14}	0.00	20300	16
$C_7H_6 + H \rightarrow C_7H_7$	(R17)	8.82×10^{8}	1.20	–2018	16
$C_7H_6 + H \rightarrow c\text{-}C_5H_5 + C_2H_2$	(R18)	3.00×10^{14}	0.00	0.00	*d*
$C_8H_{10} \rightarrow b\text{-}C_7H_7 + CH_3$	(R19)	6.00×10^{15}	0.00	75000	42
$C_9H_7 + O = C_6H_5\text{–}CHCH + CO$	(R20)	1.00×10^{14}	0.00	0.00	33
$C_6H_5 + C_2H_2 = C_8H_6 + H$	(R21)	8.32×10^{22}	–2.68	17400	23

TABLE 1: Continued

reactions		$k = AT^n \exp(-E_a/RT)$ units: mol, s, cm^3 A	n	E_a cal/mol	refs
c-$C_5H_5 + c$-$C_5H_5 \rightarrow$ 1-$C_{10}H_9 + H$	(R22)	2.00×10^{13}	0.00	4000	33
1-$C_{10}H_9 \rightarrow$ 2-$C_{10}H_9$	(R23)	3.82×10^{12}	–1.92	6015	*e*
2-$C_{10}H_9 \rightarrow$ 1-$C_{10}H_9$	(R24)	5.13×10^{13}	–3.38	–3386	*e*
2-$C_{10}H_9 \rightarrow$ 3-$C_{10}H_9$	(R25)	3.47×10^{22}	–4.77	14773	*e*
3-$C_{10}H_9 \rightarrow$ 2-$C_{10}H_9$	(R26)	6.70×10^{21}	–4.65	29528	*e*
3-$C_{10}H_9 \rightarrow$ 4-$C_{10}H_9$	(R27)	1.36×10^{14}	–2.37	7479	*e*
4-$C_{10}H_9 \rightarrow$ 3-$C_{10}H_9$	(R28)	7.14×10^{14}	–2.4	–254	*e*
4-$C_{10}H_9 \rightarrow$ c-$C_{10}H_9$	(R29)	5.49×10^{11}	–1.67	5136	*e*
c-$C_{10}H_9 \rightarrow$ 4-$C_{10}H_9$	(R30)	2.10×10^{11}	–1.52	29884	*e*
c-$C_{10}H_9 \rightarrow C_{10}H_8 + H$	(R31)	7.16×10^{10}	0.76	15144	*e*
$C_{10}H_8 + H \rightarrow c$-$C_{10}H_9$	(R32)	4.43×10^{8}	1.54	11108	*e*
b-$C_7H_7 + C_3H_3 = C_6H_5$–CHCHCCH$_2$ + H	(R33)	6.00×10^{11}	0.00	0.00	12
C_6H_5–CHCHCHCH = C_6H_5–CHCHCCH$_2$	(R34)	3.56×10^{10}	0.88	37300	*f*
C_6H_5–CHCHCHCH $\rightarrow$ c-$C_{10}H_9$	(R35)	2.17×10^{9}	–0.83	1555	*e*
c-$C_{10}H_9 \rightarrow C_6H_5$–CHCHCHCH	(R36)	1.33×10^{11}	–0.55	38522	*e*

[a] Deduced from Lifshitz et al.[25] and the branching ratio analysis of Eng et al.[26] [b] Deduced from the total O+C_6H_6 rate constant of Ko et al.[44] and the branching ratio analysis of Nguyen et al.[45] [c] From Jones et al.[28] with the pre-exponential factor times by 2 (see text). [d] Estimated (see text). [e] RRKM computations for 36 Torr. Input parameters come from Kislov et al.[39] [f] By analogy with n-C_3H_7 = i-C_3H_7.[47]

In summary, toluene is consumed through two main pathways presented in scheme 1. The first (path A) produces benzene and phenyl radical and the second forms the benzyl radical (path B).

2. Further Reactions of Benzene and Phenyl Radical (Path A). As shown in Figure 7, benzene (C_6H_6) is a major intermediate in toluene combustion. Recently, Li and coworkers[15] made the same observation in a similar toluene flame with an equivalence ratio of 1.9. The benzene mole fraction profile is well predicted by the mechanism. Its main consumption pathways lead to phenyl radical production through H abstraction reactions by H atom (R6; 52%), by OH radical (R7; 38%) and by O atom (R8; 3%). At last, 3% of benzene is converted to phenol by reaction with OH radical R9 and 4% reacts with O atom to produce phenoxy radical and H atom R10.

$$C_6H_6 + H = C_6H_5 + H_2 \quad (R6)$$

$$C_6H_6 + OH = C_6H_5 + H_2O \quad (R7)$$

$$C_6H_6 + O = C_6H_5 + OH \quad (R8)$$

$$C_6H_6 + OH = C_6H_5OH + H \quad (R9)$$

$$C_6H_6 + O = C_6H_5O + H \quad (R10)$$

Phenyl radical (C_6H_5) mainly reacts with O_2 to produce either phenoxy radical (C_6H_5O) or benzoquinone ($C_6H_4O_2$) by reactions

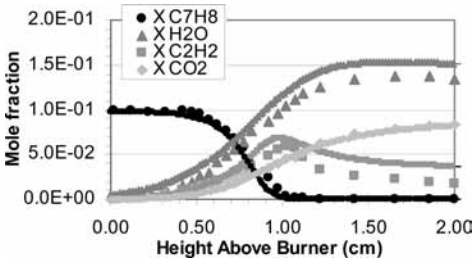

Figure 4. Gas chromatography measurements (symbols) and predicted mole fraction profiles (curves with symbols) of toluene (C_7H_8), water (H_2O), acetylene (C_2H_2), and carbon dioxide (CO_2).

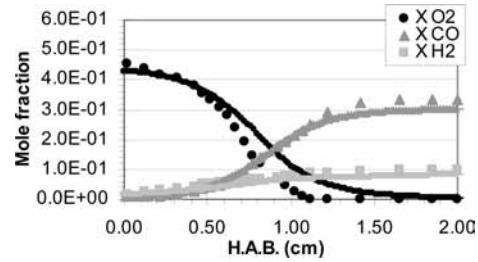

Figure 5. Gas chromatography measurements (symbols) and predicted mole fraction profiles (curves with symbols) of molecular oxygen (O_2), carbon monoxide (CO) and molecular hydrogen (H_2).

R11 and R12, respectively. The branching ratio between phenoxy and benzoquinone pathways has been taken from the work of Kumaran and Michael.[27] Additional phenyl consumption routes lead to linear hex-3-en-1,5-diyne (C_6H_4) (23%) and i-C_4H_3 production (3%).

$$C_6H_5 + O_2 = C_6H_5O + O \quad \text{(R11)}$$

$$C_6H_5 + O_2 = C_6H_4O_2 + H \quad \text{(R12)}$$

$$C_6H_5O = c\text{-}C_5H_5 + CO \quad \text{(R13)}$$

The phenoxy radical, formed from benzene and phenyl radical, dissociates into carbon monoxide and the resonantly stabilized cyclopentadienyl radical (c-C_5H_5) through reaction R13. As discussed below, unlike in benzene combustion,[22,23] the phenoxy channel is not the only c-C_5H_5 production route in toluene flames.

3. Further Reactions of Benzyl Radical: A C_7H_6 Pathway? (Path B). Benzyl radical (b-C_7H_7) consumption pathways are not well-defined in the literature. Indeed some groups recommend its degradation into c-$C_5H_5 + C_2H_2$ and $C_4H_4 + C_3H_3$[12] and others suggest pathways leading to c-$C_5H_5 + C_2H_2$ and $C_7H_6 + H$.[28] In 1997 Jones and co-workers theoretically studied the decomposition of benzyl radical (b-C_7H_7).[28] They concluded that the ring-opening channel forming a linear l-C_7H_7 radical and the pathway producing 1,3-cyclopentadiene-5-vinyl radical (C_7H_7) are the main benzyl degradation routes. Jones and co-workers suggested that C_7H_7 is decomposed into c-$C_5H_5 + C_2H_2$ either directly or by an H-fission into 1,3-cyclopentadiene-5-ethynyl followed by an H addition to displace acetylene.[28] Recently, Cavallotti and co-workers have reinvestigated the C_7H_7 potential energy surface.[16] Whereas their conclusions are similar to those of Jones et al.[28] until the 1,3-cyclopentadiene-5-vinyl radical, they have suggested that C_7H_7 decomposes to fulvenallene + H rather than to cyclopentadiene-5-ethynyl + H. Then, they proposed an approximation of the rate constant for the overall $C_7H_6 + H \rightarrow C_5H_5 + C_2H_2$ reaction: $k = 1.06 \times 10^8\ T^{1.35} \exp(1716/T)$ cm^3 mol^{-1} s^{-1}. Very recently, da Silva and co-workers have theoretically confirmed that fulvenallene and H are the primary products of the benzyl radical thermal decomposition.[17] They stressed that other pathways as the ring-opening channel should not compete with the fulvenallene formation.

Rate coefficients of reactions R14 and R15 have been taken from Jones et al.,[28] as presented in Table 1.

$$b\text{-}C_7H_7 \rightarrow C_7H_7 \quad \text{(R14)}$$

$$C_7H_7 \rightarrow b\text{-}C_7H_7 \quad \text{(R15)}$$

The pre-exponential factor of reaction R14 has been multiplied by a factor of 2. This adjustment is coherent either with experimental measurements and uncertainties associated with their theoretical predictions[28] or with the lowest activation energy proposed by Cavallotti and co-workers for R14.[16]

According to the recent theoretical findings presented above, the C_7H_6 chemical structure of our model corresponds to fulvenallene.

$$C_7H_7 \rightarrow C_7H_6 + H \quad \text{(R16)}$$

$$C_7H_6 + H \rightarrow C_7H_7 \quad \text{(R17)}$$

$$C_7H_6 + H \rightarrow c\text{-}C_5H_5 + C_2H_2 \quad \text{(R18)}$$

Rate parameters of the reaction R16 are deduced from Cavallotti et al.[16] In their work, the authors found that the 1,3-cyclopentadiene-5-vinyl radical (C_7H_7) can decompose into fulvenallene either by a direct C−H bond fission or by two two-step processes based on an H transfer reaction followed by a C−H bond fission. Since they stressed that the direct pathway was too slow to explain experimental evidence, rate parameters corresponding to a two-step channel have been chosen for reaction R16. Among two-step pathways that Cavalotti and co-workers analyzed, the one with the lowest H atom transfer activation energy (20.3 kcal/mol) has been chosen. It corresponds to an H atom transfer from the tertiary hydrogen atom of the C_5 ring (see position of C_7H_7 in Scheme 1) to a vicinal CH group (see position of C_7H_7 in Scheme 1). Since authors did not propose a pre-exponential factor for this reaction, we use the one calculated for the same H atom transfer but to the CCH_2 group of the C_7H_7. Cavalotti and co-workers expected that the subsequent C−H bond fission should proceed quite fast and should consequently not be a rate determining step. Rate parameters of the reverse reaction R17 are assumed to be similar to those suggested in Cavallotti et al.[16] for the reaction between fulvenallene and H giving benzyl radical.

When included in our model, the rate parameters of Cavallotti and co-workers[16] for R18 were unable to predict the measured cyclopentadiene (C_5H_6) maximum mole fraction of this work. However, in their study, the authors highlight that this rate constant should be underestimated.[16] Then, we propose a new order of magnitude for the rate constant of reaction R18 by fitting its pre-exponential factor to a value able to predict the experimental cyclopentadiene mole fraction (C_5H_6): $k_{18} = 3.0\ 10^{14}$ cm^3 mol^{-1} s^{-1}.

In Scheme 1, the kinetic analysis shows that the benzyl radical (b-C_7H_7) is mainly converted to C_7H_7. Minor pathways produce naphthalene ($C_{10}H_8$), indene (C_9H_8), and ethylbenzene (C_8H_{10}). C_7H_7 is converted to C_7H_6, followed by an H addition yielding c-$C_5H_5 + C_2H_2$. The toluene submechanism developed in the

SCHEME 1: Main Reaction Pathways of Toluene Consumption[a]

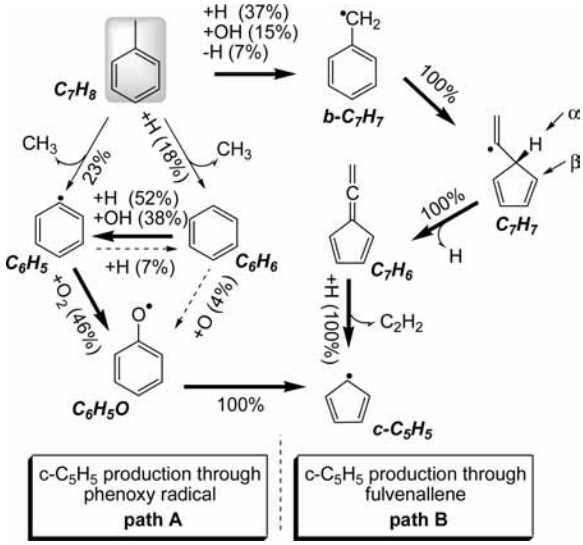

[a] Percentages represent the reaction contribution to the consumption of each compound. Bold arrows indicate the main pathways.

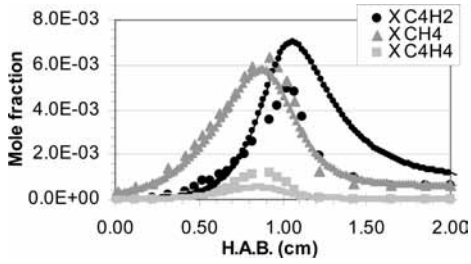

Figure 6. Gas chromatography measurements (symbols) and predicted mole fraction profiles (curves with symbols) of diacetylene (C_4H_2), methane (CH_4), and vinylacetylene (C_4H_4).

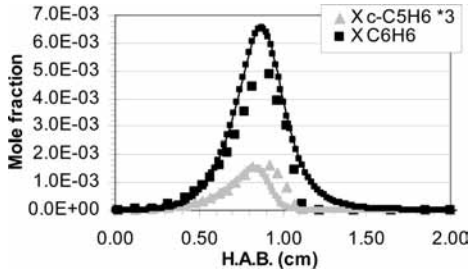

Figure 7. Gas chromatography measurements (symbols) and predicted mole fraction profiles (curves with symbols) of benzene (C_6H_6) and cyclopentadiene (c-C_5H_6). Experimental and predicted c-C_5H_6 profiles are multiplied by a factor 3.

present work well predicts toluene (C_7H_8), benzene (C_6H_6), cyclopentadiene (c-C_5H_6), and acetylene (C_2H_2) gas chromatography measurements (Figures 4 and 7) and MBMS mole fraction profiles corresponding to m/z ratios of C_7H_7 and C_7H_6 (Figure 8). Whereas we are not able to experimentally confirm the structure of C_7H_6, we show that a kinetic model based on recent theoretical findings on benzyl radical degradation to cyclopentadienyl radical and acetylene through a fulvenallene intermediate leads to a very close prediction of MBMS mole fraction measurements of C_7H_7 and C_7H_6 m/z ratios in a rich toluene flame.

Moreover, if this pathway is removed from the kinetic model, we are unable to predict the experimental cyclopentadiene maximum mole fraction, mainly produced from c-C_5H_5 and H

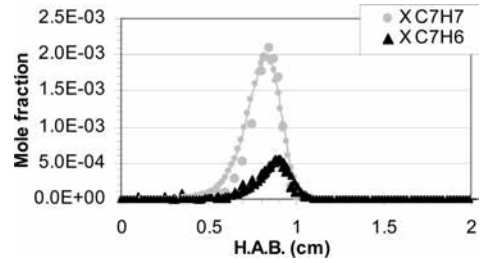

Figure 8. Molecular beam mass spectrometry measurements (symbols) and predicted mole fraction profiles (curves with symbols) of m/z = 91 (C_7H_7) and m/z = 90 (C_7H_6).

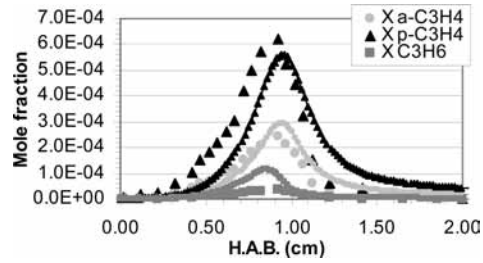

Figure 9. Gas chromatography measurements (symbols) and predicted mole fraction profiles (curves with symbols) of allene (a-C_3H_4), propyne (p-C_3H_4), and propylene (C_3H_6).

recombination. Indeed, kinetic modeling predicts that only 31% of c-C_5H_5 comes from the phenoxy radical decomposition channel (path A, see scheme 1) and 61% is formed from the C_7H_6 pathway (path B).

4. Reactions of the Cyclopentadienyl Radical. In former kinetic models on aromatic hydrocarbon oxidation, the cyclopentadienyl radical was mainly converted into cyclopentadienone (C_5H_4O) by reaction with O atom.[22,23,29,30] However, in a recent extensive flow reactor oxidation study of c-C_5H_5, Butler and Glassman[31] have shown that the major cyclopentadienyl radical oxidation route goes through the 2,4-cyclopentadienoxy radical (C_5H_5O) formation, followed by a ring-opening to yield n-C_4H_5 + CO rather than C_5H_4O. Kinetic parameters for C_5H_5O consumption suggested in their work have been included in our kinetic model. According to the numerical simulation, 88% of the c-C_5H_5 radical produces acetylene and propargyl radicals (C_3H_3) by unimolecular dissociation, 9% recombines with an H atom forming c-C_5H_6, and 1% reacts with O or HO_2 producing 2,4-cyclopentadienoxy radical (C_5H_5O). Then, 2% of c-C_5H_5 recombines toward polycyclic aromatic hydrocarbons formation, as discussed further.

The cyclopentadiene mole fraction profile is well predicted by the model (Figure 7) and c-C_5H_6 consumption mainly yields back to c-C_5H_5 by H abstraction reactions with either H atom (52%), OH radical (12%), or O atom (10%). c-C_5H_6 decomposition channels linking C_5 to C_3H_4 chemistry proposed in the theoretical work of Backsay and Mackie[32] have been included in our kinetic model. This addition together with the use of the rate constant expression proposed by Richter and Howard for the pressure dependent reaction $C_2H + CH_3 = p$-C_3H_4 leads to allene (a-C_3H_4) and propyne (p-C_3H_4) mole fraction profiles close to the experiment (Figure 9).

Vinylacetylene (C_4H_4) production which comes from the degradation of C_5H_4O and c-C_5H_5O, mainly produced from benzoquinone decomposition, is slightly underpredicted by the mechanism (figure 6). Predicted mole fractions of diacetylene and propylene are close to the experimental measurements (Figures 6 and 9, respectively).

5. Formation of Larger Chemical Species and PAH. In the present kinetic model, styrene (C_8H_8) is produced through

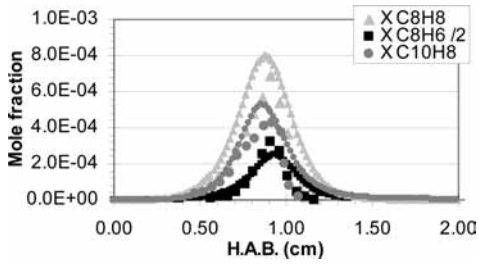

Figure 10. Gas chromatography measurements (symbols) and predicted mole fraction profiles (curves with symbols) of styrene (C_8H_8), phenylacetylene (C_8H_6), and naphthalene ($C_{10}H_8$). Experimental and predicted C_8H_6 profiles are divided by a factor 2.

two channels. In the first pathway R19, CH_3 and benzyl radicals recombine to produce ethylbenzene (C_8H_{10}) which is involved in styrene formation through $C_6H_5-CHCH_3$ and $C_6H_5-CH_2CH_2$ intermediates.

$$C_8H_{10} = b\text{-}C_7H_7 + CH_3 \qquad \text{(R19)}$$

Since this channel alone was not able to explain the styrene maximum mole fraction measured in the toluene flame, a second pathway has been added. It consists of an O atom addition on the indenyl radical (C_9H_7), followed by a dissociation to C_6H_5-CHCH radical R20, involved in styrene formation.

$$C_9H_7 + O \rightarrow C_6H_5 - CHCH + CO \qquad \text{(R20)}$$

The rate constant parameters of this O addition R20 have been taken from the kinetic model of Marinov and co-workers[33] and lead to a good prediction of styrene mole fraction profile (figure 10). Phenylacetylene (C_8H_6) mole fraction profile is well predicted by the kinetic model (figure 10). Its formation is considered through acetylene addition to phenyl radical followed by an H elimination R21.

$$C_6H_5 + C_2H_2 = C_8H_6 + H \qquad \text{(R21)}$$

Naphthalene ($C_{10}H_8$) formation is considered either through cyclopentadienyl radicals self-recombination,[33–36] hydrogen abstraction C_2H_2 addition (HACA),[37] or benzyl and propargyl recombination.[12] Whereas $C_{10}H_8$ formation routes are generally introduced as global and nonelementary reactions in many kinetic models, a particular attention was paid to describe these reactions as elementary steps.

In the present work, we use rate parameters proposed by Marinov and co-workers[33] ($c\text{-}C_5H_5 + c\text{-}C_5H_5 \rightarrow C_{10}H_8 + 2H$; $k = 2.0 \times 10^{13} \exp(-2013/T)$ cm^3 mol^{-1} s^{-1}) for the recombination of two c-C_5H_5 producing the $C_5H_5-C_5H_4$ radical (1-$C_{10}H_9$) and H.

$$c\text{-}C_5H_5 + c\text{-}C_5H_5 \rightarrow 1\text{-}C_{10}H_9 + H \qquad \text{(R22)}$$

Then the $C_5H_5-C_5H_4$ radical isomerizes to $C_{10}H_8 + H$ on a $C_{10}H_9$ potential energy surface according to the recent theoretical study of Kislov and Mebel[38] (see Scheme 2 and reactions R23−R32 in Table 1). The HACA pathway[36] has been implemented in our mechanism by using the kinetic scheme investigated by Kislov et al.[39] The rate constant of Colket and Seery[12] is used for the reaction between benzyl (b-C_7H_7) and propargyl (C_3H_3) radicals forming the $C_6H_5-CHCHCCH_2$

SCHEME 2: Main Reaction Pathways of Naphthalene Formation[a]

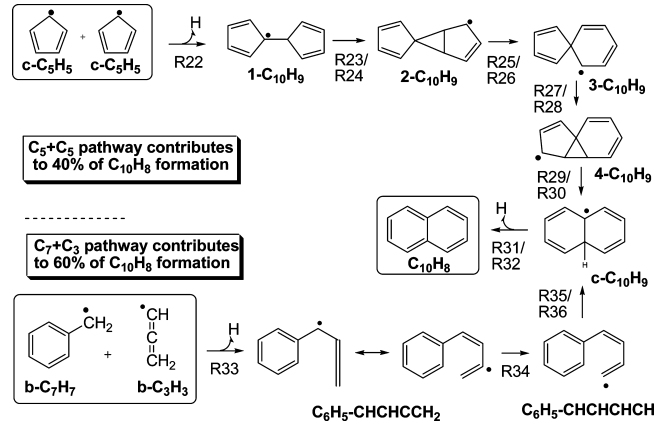

[a] Kinetic parameters of numbered reactions are reported in Table 1.

radical and H atom R33. As described in Scheme 2, after an isomerization to $C_6H_5-CHCHCHCH$ R34 and a cyclization to c-$C_{10}H_9$ (R35 and R36), this radical is involved into the reaction scheme of cyclopentadienyl self-recombination.

$$b\text{-}C_7H_7 + C_3H_3 \rightarrow C_6H_5 - CHCHCCH_2 + H \qquad \text{(R33)}$$

$$C_6H_5 - CHCHCHCH = C_6H_5 - CHCHCCH_2 \qquad \text{(R34)}$$

$$C_6H_5 - CHCHCHCH \rightarrow c\text{-}C_{10}H_9 \qquad \text{(R35)}$$

$$c\text{-}C_{10}H_9 \rightarrow C_6H_5 - CHCHCHCH \qquad \text{(R36)}$$

The naphthalene mole fraction profile is relatively well predicted by the kinetic model, as presented in Figure 10. The model predicts that two pathways compete for naphthalene production: the cyclopentadienyl radicals self-recombination accounts for 62% and the recombination between benzyl and propargyl radicals contributes to 38%, as summarized in Scheme 2. This finding confirms that as in toluene pyrolysis, the b-C_7H_7 + C_3H_3 radicals recombination is an important naphthalene formation channel in flames.

Similarly to benzene, naphthalene reacts either by H abstraction reactions forming naphtyl radicals (1-$C_{10}H_7$ and 2-$C_{10}H_7$) or by O addition producing naphthoxy radicals (1-$C_{10}H_7O$ and 2-$C_{10}H_7O$). 1-$C_{10}H_7$ and 2-$C_{10}H_7$ recombine with methyl radical producing, respectively, 1 and 2-methyl naphthalene (1-$C_{11}H_{10}$ and 2-$C_{11}H_{10}$) or react with O_2 forming naphtoxy radicals and O atoms. Experimental mole fraction profiles of both methyl naphthalene isomers are well predicted by the kinetic model, as shown in figure 11. Naphthoxy radicals (1-$C_{10}H_7O$ and 2-$C_{10}H_7O$) dissociate into CO and indenyl radical (C_9H_7).

In the present kinetic model, indene (C_9H_8) is produced from cyclopentadienyl radicals recombination or by reaction between benzyl radical and C_2H_2 as proposed by Kislov and Mebel.[38] The model predicts an indene maximum mole fraction of 7.96×10^{-4}. Although we were unable to follow this species by GC, this value is of the same magnitude as a measurement performed by Li and co-workers[16] (8.0×10^{-4}) in a flame with a composition close to the one investigated in this work.

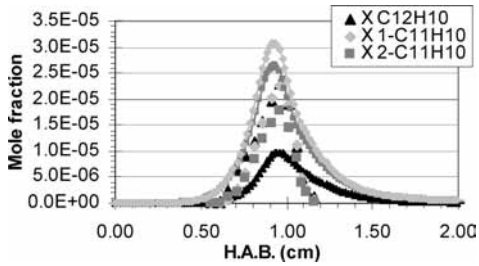

Figure 11. Gas Chromatography measurements (symbols) and predicted mole fraction profiles (curves with symbols) of biphenyl ($C_{12}H_{10}$), 1-methylnaphthalene (1-$C_{11}H_{10}$) and 2-methylnaphthalene (2-$C_{11}H_{10}$).

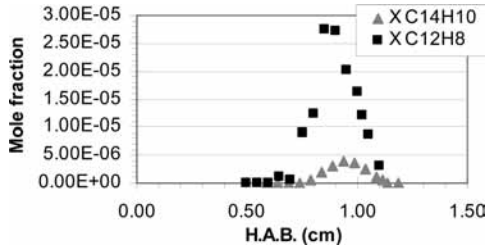

Figure 12. Gas chromatography measurements of phenanthrene ($C_{14}H_{10}$, represented by triangles) and acenaphthylene ($C_{12}H_8$, represented by squares).

Nevertheless, further indene measurements are necessary to validate the C_9H_8 reaction pathway used in our model.

As shown in Figure 11, biphenyl ($C_{12}H_{10}$) is underestimated by the kinetic model. $C_{12}H_{10}$ is mainly produced from phenyl radicals recombination.

Mole fraction profiles of phenanthrene ($C_{14}H_{10}$) and acenaphthylene ($C_{12}H_8$) have been measured (Figure 12), but reaction paths leading to their production are not included in the present kinetic model. The extension of the mechanism to larger PAH and soot formation will be the subject of future works.

Conclusions

An experimental investigation of a rich, one-dimensional, premixed and laminar toluene flame was performed at low pressure (36 Torr). Mole fraction profiles of 23 chemical species were measured by gas chromatography. Since recent theoretical studies have identified C_7H_7 and C_7H_6 as key species in toluene combustion, mole fraction profiles of *m*/*z* ratios corresponding to these both compounds have been measured by molecular beam mass spectrometry.

A kinetic model with a good predictive capability including a recent literature survey on critical steps of aromatic oxidation such as cyclopentadiene oxidation, benzyl radical decomposition and naphthalene formation has been developed. Main toluene combustion pathways have been determined by an extensive flow rate analysis of predicted data. According to the numerical simulation, benzene, phenyl and benzyl radicals are major products of the toluene consumption. Phenyl radical and benzene lead to cyclopentadienyl production through the well-known phenoxy channel while benzyl radical is mainly consumed into fulvenallene (C_7H_6), giving cyclopentadienyl radical and acetylene by reaction with H atom.

Gaseous chromatography measurements of toluene, benzene, cyclopentadiene, acetylene and MBMS mole fraction profiles of *m*/*z* ratios corresponding to C_7H_7 and C_7H_6 compounds are in very close agreement with model predictions. This finding confirms recent theoretical studies on benzyl decomposition to cyclopentadienyl and acetylene through a C_7H_6 pathway. Whereas the model considers C_7H_6 as fulvenallene, its chemical structure could not be confirmed using the experimental techniques of the present work.

Maximum mole factions of PAH precursors as *c*-C_5H_6, C_2H_2, and C_3H_4 isomers are well predicted and calculated mole fractions of naphthalene and methylnaphthalene isomers are close to the experiment. Cyclopentadienyl radicals recombination competes with the benzyl + propargyl radical addition for naphthalene formation.

For the first time, a kinetic model including a C_7H_6 chemical species has been validated against experimental data of a toluene-oxygen-argon premixed, laminar and one-dimensional flame. This kinetic mechanism will help further works on PAH formation and could be useful for future modeling of soot formation in toluene combustion.

Acknowledgment. V.D. is grateful to the F.RIA (Fonds pour la formation à la Recherche dans l'Industrie et dans l'Agriculture) for financial support.

Supporting Information Available: Full C_5 to C_{12} kinetic submechanism including thermochemical and transport properties of its chemical species. This material is available free of charge via the Internet at http://pubs.acs.org.

References and Notes

(1) Dockery, D. W.; Pope, C. A.; Xu, X.; Spengler, J. D.; Ware, J. H.; Fay, M. E.; Ferris, B. G.; Speizer, F. E. *New England J. Med.* **1993**, *329*, 1753.

(2) McEnally, C. S.; Pfefferle, L. D.; Atakan, B.; Kohse-Höinghaus, K. *Prog. Energy Combust. Sci.* **2006**, *32*, 247.

(3) Venkat, C.; Brezinsky, K.; Glassman, I. *Proc. Combust. Inst.* **1982**, *19*, 143.

(4) Emdee, J. L.; Brezinsky, K.; Glassman, I. *J. Phys. Chem.* **1992**, *96*, 2151.

(5) Brezinsky, K.; Litzinger, T. A.; Glassman, I. *Int. J. Chem. Kinet.* **1984**, *27*, 337.

(6) Brezinsky, K. *Prog. Energy Combust. Sci.* **1986**, *12*, 1.

(7) Dagaut, P.; Pengloan, G.; Ristori, A. *Phys. Chem. Chem. Phys.* **2002**, *4*, 1846.

(8) Bounaceur, R.; Da Costa, I.; Fournet, R.; Billaud, F.; Battin-Leclerc, F. *Int. J. Chem. Kinet.* **2005**, *37*, 25.

(9) Sivaramakrishnan, R.; Tranter, R. S.; Brezinsky, K. *Combust. Flame* **2004**, *139*, 340.

(10) Sivaramakrishnan, R.; Tranter, R. S.; Brezinsky, K. *Proc. Combust. Inst.* **2005**, *30*, 1165.

(11) Pamidimukkala, K. M.; Kern, R. D.; Patel, M. R.; Wei, H. C.; Kiefer, J. H. *J. Phys. Chem.* **1987**, *91*, 2148.

(12) Colket, M. B.; Seery, D. J. *Proc. Combust. Inst.* **1994**, *25*, 883.

(13) Hamins, A.; Seshadri, K. *Combust. Flame* **1987**, *68*, 295.

(14) Bakali, A.; Dupont, L.; Lefort, B.; Lamoureux, N.; Pauwels, J. F.; Montero, M. *J. Phys. Chem. A* **2007**, *111*, 3907.

(15) Li, Y.; Zhang, L.; Tian, Z.; Yuan, T.; Wang, J.; Yang, B.; Qi, J. *Energy Fuels* **2009**, *23*, 1473.

(16) Cavallotti, C.; Derudi, M.; Rota, R. *Proc. Comb. Inst.* **2009**, *32*, 115.

(17) Da Silva, G.; Cole, J. A.; Bozzelli, J. W. *J. Phys. Chem. A* **2009**, *113*, 6111.

(18) Detilleux, V.; Vandooren, J. *Combust. Sci. Technol.* **2008**, *180*, 1347.

(19) Mahnen, G. Contribution à l'étude du mécanisme des déflagrations. Ph.D. Dissertation, Université Catholique de Louvain, Belgium, 1973.

(20) Kent, J. H. *Combust. Flame* **1970**, *14*, 279.

(21) Konnov, A. A. *Combust. Flame* **2008**, *152*, 507.

(22) Ristori, A.; Dagaut, P.; El Bakali, A.; Pengloan, G.; Cathonnet, M. *Combust. Sci. Technol.* **2001**, *167*, 223.

(23) Richter, H.; Howard, J. B. *Phys. Chem. Chem. Phys.* **2002**, *4*, 2038.

(24) COSILAB, The Combustion Simulation Laboratory Version 2.0.8. 2007, Rotexo GmbH & Co. KG. Haan (Germany) www.SoftPredict.com.

(25) Lifshitz, A.; Suslensky, A.; Tamburu, C. *Proc. Combust. Inst.* **2000**, *28*, 1733.

(26) Eng, R. A.; Gebert, A.; Goos, E.; Hippler, H. *Phys. Chem. Chem. Phys.* **2002**, *4*, 3989.

(27) Kumaran, S. S.; Michael, J. V. *Proc 21st International Symposium on Shock Waves*; Great Keppel Island: Australia, 1997; paper 6510, pp 241−244.
(28) Jones, J.; Backsay, G. B.; Mackie, J. C. *J. Phys. Chem. A* **1997**, *101*, 7105.
(29) Alzueta, M. U.; Glarborg, P.; Dam-Johansen, K. *Int. J. Chem. Kinet.* **2000**, *32*, 498.
(30) Costa, I. D.; Fournet, R.; Billaud, F.; Battin-Leclercl, F. *Int. J. Chem. Kinet.* **2003**, *35*, 503.
(31) Butler, R.; Glassman, I. *Proc. Combust. Inst.* **2009**, *32*, 395.
(32) Bacskay, G. B.; Mackie, J. C. *Phys. Chem. Chem. Phys.* **2001**, *3*, 2467.
(33) Marinov, N. M.; Pitz, W. J.; Westbrook, C. K.; Castaldi, M. J.; Senkan, S. M. *Combust. Sci. Technol.* **1996**, *116*, 211.
(34) Dean, A. M. *J. Phys. Chem.* **1990**, *94*, 1432.
(35) Melius, C. F.; Colvin, M. E.; Marinov, N. M.; Pitz, W. J.; Senkan, S. M. *Proc. Combust. Instit.* **1996**, *26*, 685.
(36) Marinov, N. M.; Pitz, W. J.; Westbrook, C. K.; Vincitore, A. M.; Castaldi, M. J.; Senkan, S. M. *Combust. Flame* **1998**, *114*, 192.
(37) Frenklach, M. *Phys. Chem. Chem. Phys.* **2002**, *4*, 2028.
(38) Kislov, V. V.; Mebel, A. M. *J. Phys. Chem. A* **2008**, *112*, 700.
(39) Kislov, V. V.; Islamova, N. I.; Kolker, A. M.; Lin, S. H.; Mebel, A. M. *J. Chem. Theory Comput.* **2005**, *1*, 908.
(40) Hippler, H.; Reihs, C.; Troe, J. *Z. Phys. Chem.* **1990**, *167*, 1.
(41) Seta, T.; Nakajima, M.; Miyoshi, A. *J. Phys. Chem. A* **2006**, *110*, 5081.
(42) Baulch, D. L.; Cobos, C. J.; Cox, R. A.; Frank, P.; Hayman, G.; Just, T.; Kerr, J. A.; Murrells, T.; Pilling, M. J.; Troe, J.; Walker, R. W.; Warnatz, J. *J. Phys. Chem. Ref. Data* **1994**, *23*, 847.
(43) Mebel, A. M.; Lin, M. C.; Yu, T.; Morokuma, K. *J. Phys. Chem. A* **1997**, *101*, 3189.
(44) Ko, T.; Adusei, G. Y.; Fontijn, A. *J. Phys. Chem.* **1991**, *95*, 8745.
(45) Nguyen, T. L.; Peeters, J.; Vereecken, L. *J. Phys. Chem. A* **2007**, *111*, 3836.
(46) Lin, C.-Y.; Lin, M. C. *J. Phys. Chem.* **1986**, *90*, 425.
(47) Matheu, D. M.; Green, W. H.; Grenda, J. M. *Int. J. Chem. Kinet.* **2003**, *35*, 95.

JP905954G